IOP Publishing Journal of Physics: Condensed Matter

J. Phys.: Condens. Matter **30** (2018) 335501 (11pp) https://doi.org/10.1088/1361-648X/aad2bf

Structural evolution and magnetic properties of anionic clusters Cr_2Ge_n ($n = 3$–14): photoelectron spectroscopy and density functional theory computation

Xiaoqing Liang[1,3], **Xiangyu Kong**[2], **Sheng-Jie Lu**[2], **Yingying Huang**[1], **Jijun Zhao**[1], **Hong-Guang Xu**[2], **Weijun Zheng**[2] and **Xiao Cheng Zeng**[3,4]

[1] Key Laboratory of Materials Modification by Laser, Ion and Electron Beams, Dalian University of Technology, Ministry of Education, Dalian 116024, People's Republic of China
[2] Beijing National Laboratory for Molecular Science, State Key Laboratory of Molecular Reaction Dynamics, Institute of Chemistry, Chinese Academy of Sciences, Beijing 100190, People's Republic of China
[3] Department of Chemistry, University of Nebraska, Lincoln, NE 68588, United States of America
[4] Department of Physics and Department of Mechanical & Materials Engineering, University of Nebraska, Lincoln, NE 68588, United States of America

E-mail: zhaojj@dlut.edu.cn, xuhong@iccas.ac.cn and xzeng1@unl.edu

Received 15 May 2018, revised 2 July 2018
Accepted for publication 11 July 2018
Published 26 July 2018

Abstract

The structural, electronic and magnetic properties of dual Cr atoms doped germanium anionic clusters, $Cr_2Ge_n^-$ ($n = 3$–14), have been investigated by using photoelectron spectroscopy in combination with density-functional theory calculations. The low-lying structures of $Cr_2Ge_n^-$ are determined by DFT based genetic algorithm optimization. For $Cr_2Ge_n^-$ with $n \leqslant 8$, the structures are bipyramid-based geometries, while $Cr_2Ge_9^-$ cluster has an opening cage-like structure, and the half-encapsulated structure is gradually covered by the additional Ge atoms to form closed-cage configuration with one Cr atom interior for $n = 10$ to 14. Meanwhile, the two Cr atoms in $Cr_2Ge_n^-$ clusters tend to form a Cr–Cr bond rather than be separated. Interestingly, the magnetic moment of all the anionic clusters considered is 1 μ_B. Almost all clusters exhibit antiferromagnetic Cr–Cr coupling, except for two clusters, $Cr_2Ge_5^-$ and $Cr_2Ge_6^-$. To our knowledge, the $Cr_2Ge_n^-$ cluster is the first kind of transition-metal doped semiconductor clusters that exhibit relatively stable antiferromagnetism within a wide size range. The experimental/theoretical results suggest high potential to modify the magnetic behavior of semiconductor clusters through introducing different transition-metal dopant atoms.

Keywords: germanium cluster, chromium doping, photoelectron spectrum, antiferromagnetic, ferromagnetic

S Supplementary material for this article is available online

(Some figures may appear in colour only in the online journal)

1361-648X/18/335501+11$33.00

1. Introduction

Transition metal (TM) doped semiconductor clusters have been extensively investigated by experimentalists and theorists [1], not only because the TM atoms can stabilize the bare semiconductor clusters but also they can induce novel properties like magnetism. Germanium clusters, as one of the semiconductor clusters, have attracted increasing attention due in part to that germanium is a potential alternative to silicon in microelectronic industry [2, 3]. However, pure germanium clusters are chemically reactive and thus unsuitable as a building block of self-assembled materials [4]. Thus, to introduce appropriate metal dopants are beneficial to design germanium-based cluster assembled materials [5–7].

Over the past two decades, there have been many experimental and theoretical studies on single-TM doped germanium clusters, TMGe_n, for example, experimental measurements on photoelectron spectra and mass spectra for 3d-TM (Cr, Mn, Cu, Zn), 4d-TM (Y–Nb) and 5d-TM (Lu–Ta) doped Ge_n clusters [8–10]. The theoretical predictions for the atomic structures and electronic properties of WGe_n ($n = 1$–17) [11], NiGe_n ($n = 1$–20) [12], CuGe_n ($n = 2$–13) [13], $\mathrm{XGe}_{10}^{0/-}$ (X = Cu, Ag, Au) [14] and MnGe_n ($n = 2$–15) [15] clusters have been reported in early years. Recently, Zheng's group have investigated a series of single-TM (V, Co, Ru, Ti, Au, Fe) doped small sized Ge_n ($n = 2$–12) clusters [16–21] by combining the anion photoelectron spectroscopy with density-functional theory (DFT) computation, from which the structural evolution from exo- to endohedral geometries was suggested. Except for the structural evolution of TM-doped germanium clusters, the magnetism induced by the dopants is also focus of interest. For example, Tang *et al* [22] found that the magnetic moments of 3d endohedral MGe_{12} (M = Sc–Ni) clusters vary between 1 and 5 μ_B using the relativistic all-electron DFT method. Kapila *et al* [23] showed that the MnGe_n and CoGe_n ($n = 1$–13) clusters have magnetic moment of 1 or 3 μ_B, contrary to the magnetic quenching in MnSi_n ($n = 1$–15) [24] at $n \geqslant 8$ and CoSi_n ($n = 2$–14) [25] at $n = 7$. First-principles investigations also revealed that CrGe_n clusters up to $n = 13$ are magnetic with high spin multiplicity (quintet or septet) [26], whereas CrSi_n clusters are non-magnetic [27].

Based on the progress on single-TM doped semiconductor clusters described above and the experimental synthesis of TM doped semiconductor materials with different composition ratios [28–32], the multiple TM atoms doped semiconductor clusters become an interesting topic and has attracted certain attentions [33–41]. In a recent study [42], we found that dual-Fe atoms doped germanium clusters can retain high magnetic moments which is twice or three times that of single-Fe atom doped germanium clusters and ferromagnetic coupling of two Fe atoms emerge in all clusters. Since bulk Fe solid at ambient conditions is ferromagnetic while bulk Cr solid is antiferromagnetic, it is interesting to explore magnetic properties of germanium clusters doped with dual Cr atoms and then compare with those doped with dual Fe atoms. Here, we investigate the $\mathrm{Cr}_2\mathrm{Ge}_n^-$ ($n = 3$–14) clusters using anion photoelectron spectroscopy and DFT computation. To compare Cr_2 and single-Cr doped germanium clusters [43–45], the current study focuses on the growth pattern behaviors, electronic and magnetic properties of the Cr_2-doped germanium clusters with 3 to 14 Ge atoms. These clusters may serve as possible building blocks for novel cluster-assembled materials. Our most important finding is that the anionic $\mathrm{Cr}_2\mathrm{Ge}_n$ clusters have stable magnetic moment of 1 μ_B for $n = 3$–14, and the interaction between two Cr atoms in most clusters is antiferromagnetically coupled, in stark contrast to Fe–Fe ferromagnetic coupling in $\mathrm{Fe}_2\mathrm{Ge}_n$ clusters [42].

2. Experimental and theoretical methods

2.1. Experimental

The experiments were performed using a magnetic-bottle photoelectron apparatus equipped with a laser vaporization cluster source, details of which were described in previous publication [46]. Briefly, the Cr-doped germanium clusters were produced in the laser vaporization source by laser ablation of a rotating and translating disk target (13 mm diameter, Cr:Ge mole ratio 1:2) with the second harmonic (532 nm) light pulses from a Nd:YAG laser (Continuum Surelite II-10), while helium gas with ~4 atm backing pressure was allowed to expand through a pulsed valve (General Valve Series 9) into the source to cool the formed clusters. The anion clusters were extracted from the cluster beam perpendicularly and mass-analyzed with a time-of-flight mass spectrometer. The cluster anions of interest were mass-selected and decelerated before being photodetached by a 266 nm laser beam from another Nd:YAG laser (Continuum Surelite II-10). The photoelectrons were energy-analyzed by a magnetic-bottle photoelectron spectrometer. The magnetic-bottle photoelectron spectrometer had an energy resolution of $\Delta E/E \approx 4.0\%$, corresponding to about 40 meV for 1 eV kinetic energy electrons. The photoelectron spectra were calibrated with the spectra of Cu- and Au- ions taken at similar conditions.

2.2. Theoretical

We carried out an unbiased global search of the low-energy isomers of the Cr–Ge alloy clusters using a comprehensive genetic algorithm (CGA) code [47] (developed in our group) incorporated with DFT calculations (CGA-DFT). More details of CGA can be found in a review article [47]. As one of widely adopted global optimization algorithms, GA and its variations have been intensively used in cluster science [48, 49]. The validity and efficiency of the present CGA-DFT scheme have been demonstrated in our previous studies on Na–Si [50], V–Si [38, 51], Pt–Sn [52], Au–Ag [53], Si–B [54] and Fe–Ge [42] binary clusters.

Here CGA-DFT search of $\mathrm{Cr}_2\mathrm{Ge}_n^-$ ($n = 3$–14) clusters was coupled with the Vienna *ab initio* simulation package (VASP) [55, 56]. To guarantee not missing possible stable isomers, the initial spin moments of two Cr atoms were set as either ferromagnetic or antiferromagnetic to globally search the isomers for all clusters. In principle, VASP can determine the lowest-energy spin multiple state of a cluster spontaneously from a set of initial spin moments for each atom. For this charged system, one extra electron was treated as a homogeneous background charge. In the GA search, sixteen initial configurations in the population were generated randomly. During each GA iteration, any two individuals were chosen as parents to produce child cluster, followed by an optional mutation operation of 50% probability. For each cluster size, we performed 1000–3000 iterations to assure high chance in locating the global minimum on the potential energy surface. We carried out spin-polarized calculations using Perdew–Burke–Enzerhof (PBE) functional [57] within the generalized gradient approximation (GGA) to optimize the child cluster structure produced in each GA iteration. During geometry optimization, we adopted coarse convergences of total energy of 10^{-4} eV and 10^{-2} eV Å^{-1} in force, respectively. The energy cutoff for the plane-wave basis was set to 400 eV. Every individual cluster was placed in a simple cubic supercell of $20 \times 20 \times 20$ Å^3 to ensure sufficient separation between the periodic images.

The geometries for all cluster isomers from the CGA-DFT search were further optimized using DFT with the PBE functional implemented in the Gaussian 09 program [58]. The 6-311+g(d) basis set was used for both Cr and Ge atoms. All geometry optimizations were performed without any symmetry constraint. As chromium has six unpaired electrons ($3d^54s^1$), many spin multiplicities were considered to account for magnetic polarization of the Cr atom. The calculated total energies were corrected by the zero-point vibrational energies. To gain insight into the charge distribution of $Cr_2Ge_n^-$, we used the Multiwfn [59] program to conduct the atomic dipole moment-corrected (ADCH) population analyses, which is an improved version of Hirshfeld charge by Lu *et al* [60]. Multiwfn was also used to analyze the partial density of states (PDOS) and molecular orbitals.

To directly compare with the experimental measurements, photoelectron spectra of anionic clusters were simulated using the 'generalized Koopman's theorem' [61] based on the energy levels from DFT calculations (see details in supplementary material) (stacks.iop.org/JPhysCM/30/335501/mmedia). Such theoretical approach has been widely verified in previous reports [38, 62–64]. A uniform Gaussian broadening of 0.08 eV was chosen for all the simulated spectra. The theoretical vertical detachment energies (VDEs) were calculated as the energy differences between the neutrals and the anions both at the geometries of anionic species, while the theoretical adiabatic detachment energies (ADEs) were calculated as the energy differences between the neutrals and the anions with the neutrals relaxed using the corresponding anions as initial structures. To verify the peaks measured in experiment, we used time-dependent DFT (TD-DFT) to calculate the excited energies of the neutral cluster by keeping the same geometry of its parent anion. We used VDE plus excited energy to transform the excited energies to the detachment energies of electrons in deep valence orbitals. To avoid the effect by the deviation of calculated VDE, we use the experimental VDE in the above definition.

The accuracy of our present DFT methodology was tested for Cr_2, Ge_2 and CrGe dimers as benchmark. The Cr_2 dimer has singlet spin multiplicity with antiferromagnetic coupling (3.3 μ_B and -3.3 μ_B for two Cr atoms), consistent with previous theoretical investigations [65–68]. Considering the well-known complexity of Cr_2 dimer, the experimental characterizations are not always consistent. The measured bond length is about 1.67 ± 0.01 Å [69–71], the binding energy is 0.71, 0.74 or 0.77 eV/atom [72–74], while the vibration frequency varies from 427.5, 470 to 480 ± 0.05 cm^{-1} [69–71]. Our calculations yield the bond length of 1.72 Å, binding energy of 0.71 eV/atom, and vibration frequency of 348 cm^{-1}, all in reasonably consistent with the experimental results. For Ge_2 dimer, the calculated bond length is 2.44 Å, in excellent agreement with the experimental value of 2.44 Å [75]; the theoretical binding energy of 1.56 eV/atom is also in line with the experimental data of 1.32 eV/atom [76]; and the vibrational frequency of 261 cm^{-1} compares reasonably well with the experimental data [77] of 286 ± 5 cm^{-1}. For CrGe dimer, our calculation yielded a quintet ground state structure with bond length of 2.44 Å, and Cr–Ge presented antiferromagnetic interaction, consistent with the previous theoretical study [26]. Its calculated binding energy is 0.87 eV/atom, which is comparable to the previous theoretical result (~1.1 eV/atom) [43], meanwhile the calculated vibration frequency is 236 cm^{-1} with lacking of experimental data for comparison. Overall, our PBE/6-311+g(d) scheme can describe the structural and bonding properties of Cr and Ge systems quite well.

3. Experimental results

The photoelectron spectra of $Cr_2Ge_n^-$ ($n = 3$–14) clusters recorded with 266 nm photons are displayed in figure S1 of supplementary material. The VDEs and ADEs of these anionic clusters determined from their photoelectron spectra are summarized in table 1. The experimental VDEs of these clusters are estimated from the maxima of the first peaks, whereas the experimental ADEs are obtained by drawing a straight line along the rising edge of the first peaks to intersect with the baseline of the experimental spectra and then adding the instrumental resolution (0.08–0.2 eV) to the electron binding energy at the intersection points.

The photoelectron spectrum of $Cr_2Ge_3^-$ exhibits four major broad peaks centered at 2.25, 3.16, 3.83, and 4.26 eV, respectively. In the spectrum of $Cr_2Ge_4^-$, there is a low-intensity peak at 2.41 eV, followed by three high-intensity broad peaks centered at 3.17, 3.59, and 3.91 eV, respectively. The spectrum of $Cr_2Ge_5^-$ displays six major peaks centered at 2.00, 3.02, 3.36, 3.66, 4.06, and 4.25 eV, respectively. As for the spectrum of $Cr_2Ge_6^-$, there is a low-intensity peak at 2.41 eV, followed by two high-intensity broad peaks at 3.07 and 4.05 eV. The spectrum of $Cr_2Ge_7^-$ has five barely distinguished peaks centered at 3.0, 3.24, 3.64, 3.92, and 4.36 eV, respectively. A low-intensity shoulder peak centered at 3.0 eV and two high-intensity broad peaks at 3.23 and 4.04 eV can be observed in the spectrum of $Cr_2Ge_8^-$.

Table 1. The low-lying isomers of $Cr_2Ge_n^-$ ($n = 3$–14) and their symmetry as well as the comparison of VDEs and ADEs in eV between theory and experiment.

				VDE (eV)		ADE (eV)	
Isomers		Sym.	Relative energy	Theo.	Expt.	Theo.	Expt.
3	A	C_s	0	2.03	2.25 ± 0.06	1.88	1.58 ± 0.08
	B	C_s	0.29	1.63		1.59	
4	A	C_s	0	2.52	2.41 ± 0.06	2.37	1.86 ± 0.08
	B	C_2	0.25	2.17		2.03	
5	A	C_{2v}	0	2.05	2.00 ± 0.06	1.87	1.77 ± 0.08
	B	C_s	0.22	2.74		2.64	
	C	C_s	0.25	2.26		2.10	
6	A	C_{2h}	0	2.27	2.41 ± 0.06	2.16	1.97 ± 0.08
	B	C_s	0.17	3.05		2.73	
	C	C_s	0.41	2.46		2.39	
7	A	C_s	0	2.63	3.0 ± 0.2	2.49	1.96 ± 0.2
	B	C_1	0.07	2.58		2.42	
	C	C_s	0.37	2.47		2.36	
8	A	C_1	0	3.11	3.0 ± 0.2	2.98	2.09 ± 0.2
	B	C_1	0.18	2.63		2.53	
9	A	C_1	0	3.02	3.0 ± 0.2	2.74	1.69 ± 0.2
	B	C_1	0.03	2.88		2.70	
	C	C_{3v}	0.21	2.90		2.84	
10	A	C_s	0	2.44	2.5 ± 0.2	2.38	2.24 ± 0.2
	B	C_s	0.14	2.60		2.55	
	C	C_1	0.24	2.93		2.72	
11	A	C_s	0	3.11	3.17 ± 0.08	2.92	2.85 ± 0.08
	B	C_1	0.27	3.20		2.98	
12	A	C_{2v}	0	2.55	3.08 ± 0.08	2.44	2.83 ± 0.08
	B	C_{2v}	0.18	2.70		2.60	
	C	C_s	0.52	2.72		2.61	
13	A	C_s	0	2.77	3.00 ± 0.08	2.66	2.76 ± 0.08
	B	C_s	0.12	2.83		2.53	
	C	C_s	0.27	2.99		2.91	
14	A	C_s	0	3.45	2.94 ± 0.08	3.36	2.71 ± 0.08
	B	C_s	0.21	3.58		3.39	
	C	C_s	0.58	3.35		3.23	
	D	C_1	0.62	2.91		2.77	

The spectrum of $Cr_2Ge_9^-$ displays a broad peak centered at 3.0 eV. The spectrum of $Cr_2Ge_{10}^-$ possesses a low-intensity peak centered at 2.5 eV, followed by a low-intensity broad peak centered at 3.03 eV and three barely resolved peaks at 3.72, 4.13, and 4.31 eV, respectively. In the spectrum of $Cr_2Ge_{11}^-$, a low-intensity peak is centered at 3.17 eV while three major peaks are centered at 3.65, 3.96, and 4.20 eV, respectively. In the spectrum of $Cr_2Ge_{12}^-$, four peaks centered at 3.08, 3.44, 3.96, and 4.29 eV, respectively, are distinguishable. The spectrum of $Cr_2Ge_{13}^-$ is similar to that of $Cr_2Ge_{12}^-$, with five major peaks centered at 3.03, 3.37, 3.77, 3.99, and 4.35 eV. The spectrum of $Cr_2Ge_{14}^-$ also has similar spectral features as that of $Cr_2Ge_{12}^-$, in which there have four major peaks centered at 2.94, 3.25, 3.75 and 4.14 eV.

4. Theoretical results

The structures of the low-lying isomers of $Cr_2Ge_n^-$ ($n = 3$–14) obtained from the CGA-DFT global search and PBE/6-311+g(d) re-optimization are displayed in figure 1, where the most stable ones are marked as A in red. Theoretical calculations of VDEs and ADEs are listed in table 1 along with the experimental results for comparison. We also simulated the photoelectron spectra of different isomers and chose the most probable ones according to their energetic stability and the main features of simulated photoelectron spectra to compare with the experimental results in figure 2. Those photoelectron spectra of isomers with higher energy from our calculation are shown in figure S2. The results of transformation from excited energies to detachment energies using TDDFT method in comparison with the experimental values are shown in table S1 for reference. In the following, we compare the theoretical results with the experimental data for each $Cr_2Ge_n^-$ cluster at a time.

4.1. $Cr_2Ge_3^-$

As shown in figure 1, the lowest-energy structure 3A and the metastable structure 3B with almost the same configuration

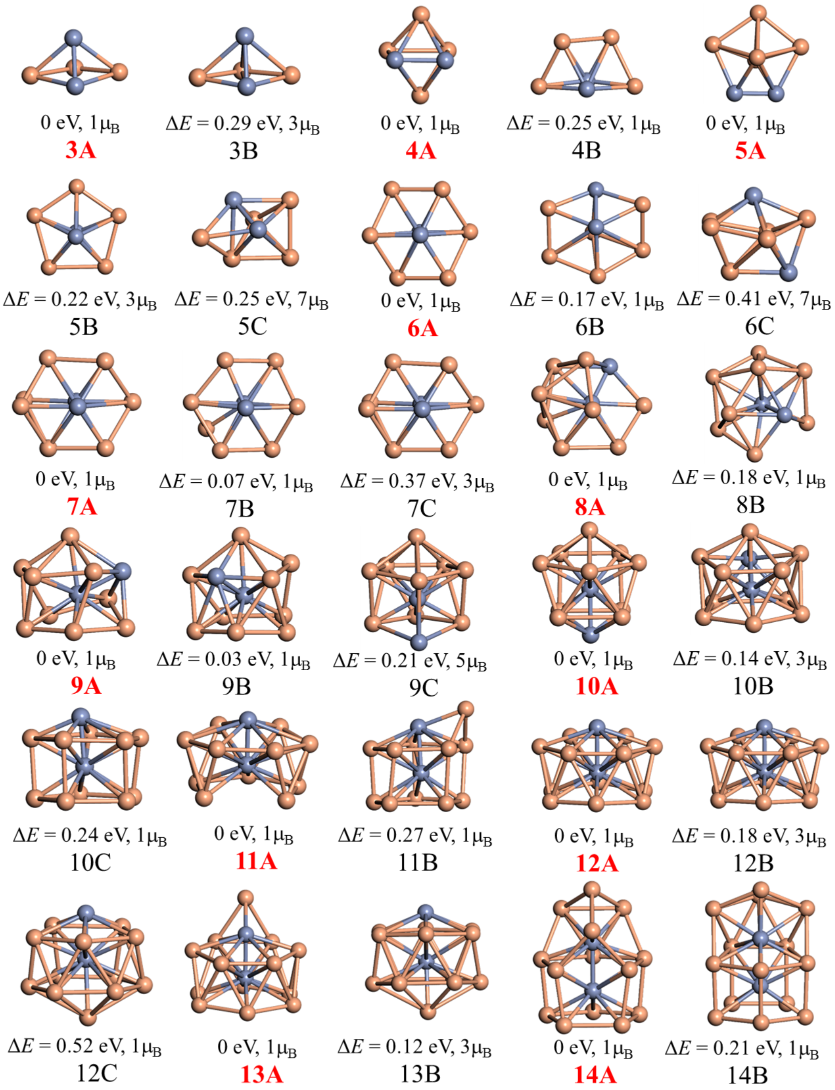

Figure 1. Equilibrium geometries of the ground state and the low-energy isomer of $Cr_2Ge_n^-$ (n = 3–14). For the isomers, the increment of total energy with respect to the ground state (in 0 eV) and total spin moment are also listed under the geometry structures. The brown (grey) balls represent germanium (chromium) atoms.

but different spin multiplicity are the two low-lying isomers of $Cr_2Ge_3^-$. Both exhibit trigonal bipyramid structures with C_s symmetry. The ground-state structure (3A) with Cr–Cr bond length of 2.10 Å has doublet spin multiplicity, i.e. total spin moment of 1 μ_B, while the metastable isomer 3B with Cr–Cr bond length of 2.12 Å and quartet spin multiplicity (3 μ_B) is 0.29 eV higher in energy. The calculated VDEs of isomers 3A and 3B are 1.96 and 1.55 eV, respectively. The VDE value of 3A is much closer to the experimental VDE (2.25 eV). In figure 2, the simulated photoelectron spectrum of isomer 3A is shown to compare with the experimental one, demonstrating the comparable peaks between theory and experiment. Thus, the experimental spectrum of $Cr_2Ge_3^-$ is most likely contributed by isomer 3A.

4.2. $Cr_2Ge_4^-$

Our calculations show that the most stable structure of $Cr_2Ge_4^-$ (4A) is a tetragonal bipyramid with Cr–Cr bond being as one side of the Cr_2Ge_2 rhombus. The 4B isomer with C_2 symmetry is a metastable structure whose energy is higher than 4A by 0.25 eV. 4A and 4B both have doublet spin multiplicity (1 μ_B). The calculated VDEs of 4A and 4B are 2.52 and 2.17 eV, respectively; the former (4A) is closer to the experimental value (2.41 eV). From the comparison of simulated and experimental spectra in figure 2, we can see the peaks are well reproduced by our theoretical calculation. Thus, we suggest isomer 4A to be the most probable one observed in experiment.

4.3. $Cr_2Ge_5^-$

For the $Cr_2Ge_5^-$ cluster, the lowest-energy configuration (5A) with doublet spin multiplicity (1 μ_B) is a pentagonal bipyramid (C_{2v} symmetry) with two Cr atoms bonded as one side of the pentagon. The metastable isomer 5B has quartet spin multiplicity (3 μ_B) is a pentagonal bipyramid with two Cr atoms capped on the vertex, and 5C is a quadrangular bipyramid with

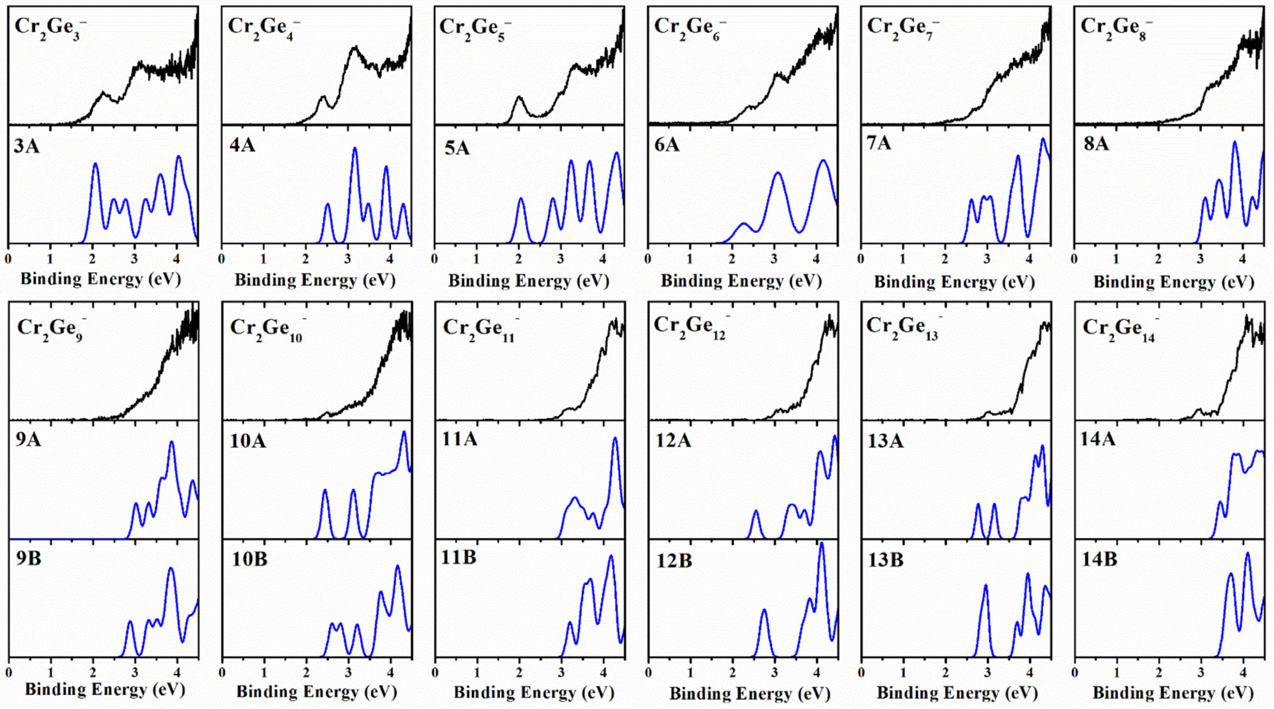

Figure 2. Simulated photoelectron spectra (blue color) and the experimental spectra (black color) for $Cr_2Ge_n^-$ ($n = 3$–14).

one extra Ge atom capped, and both isomers have C_s symmetry. 5B and 5C have spin multiplicity of quartet and octet and are less stable than 5A by 0.22 and 0.25 eV, respectively. The calculated VDEs of 5A, 5B and 5C are 2.05, 2.74 and 2.26 eV, respectively. Compared with the experimental value of 2.00 eV, the VDE of 5A is much closer than the other two isomers. From the comparison between simulated and experimental photoelectron spectra in figure 2, we suggest that 5A is the most probable one in experiment, while 5B and 5C isomers can be ruled out in the experiment.

4.4. $Cr_2Ge_6^-$

The most stable structure of $Cr_2Ge_6^-$, isomer 6A, is a non-coplanar hexagon capped by two Cr atoms like a chair-shaped configuration (see figure 1), similar to that of $V_2Si_6^-$ [46] and $Nb_2Si_6^-$ [63]. The metastable isomer 6B is generated when one Cr atom is presented in the six-membered ring, and it is 0.17 eV less stable than 6A. Both 6A and 6B correspond to doublet spin state (1 μ_B). The isomer 6C with octet spin multiplicity (7 μ_B), lying 0.41 eV higher in energy, are based on the pentagonal pyramid with two Cr atoms separated by Ge. The calculated VDEs of 6A, 6B and 6C are 2.27, 3.05 and 2.46 eV, respectively. As shown in figure 2, the three characteristic peaks observed in experiment can be reproduced by the simulated spectrum of isomer 6A, indicating that it is the most probable one in the experiment. Isomers 6B and 6C can be ruled out due to their higher energy relative to isomer 6A although the VDE of isomer 6C is close to the experimental VDE of 2.41 eV. The theoretical photoelectron spectra of isomers 6B and 6C are shown in figure S2. Through comparison with the experimental features, we note that 6B and 6C unlikely exist in the experiment.

4.5. $Cr_2Ge_7^-$

The low-lying structures of $Cr_2Ge_7^-$ are based on the hexagonal pyramid, that is, isomers 7A, 7B and 7C can be all derived from isomer 6A by adding one extra Ge atom. Isomers 7A and 7C have the same structures with different spin multiplicities, i.e. doublet for 7A (1 μ_B) and quartet for 7C (3 μ_B). Isomers 7B (doublet spin multiplicity with total spin moment of 1 μ_B) and 7C are 0.07 and 0.37 eV higher than isomer 7A in energy, respectively. The theoretical VDEs of 7A, 7B, 7C are 2.63, 2.58 and 2.47 eV, respectively. Compared with the experimental VDE (3.0 eV) and photoelectron spectra in figure 2, 7A agree well with the experimental features. Since isomer 7B is nearly degenerated with 7A, we present its photoelectron spectrum in figure S2, which indicates that 7B is probably observed in experiment. On the other hand, 7C with substantially higher energy than 7A and 7B unlikely exist in the experiment and can be ruled out.

4.6. $Cr_2Ge_8^-$

Starting from $Cr_2Ge_8^-$, the cluster isomers tend to form endohedral structures with one interior Cr atom. 8A, as the lowest-energy structure, is energetically lower than 8B by 0.18 eV and they both have doublet spin multiplicities (1 μ_B). Our calculated VDEs are 3.11 and 2.63 eV for 8A and 8B, respectively, from which 8A is closer to the experimental VDE of 3.0 eV. After comparing the simulated photoelectron spectra in figure 2 with the measured one, we predict 8A is the most probable one in experiment.

4.7. $Cr_2Ge_9^-$

The low-energy isomers of $Cr_2Ge_9^-$ are all endohedral structures with one Cr atom at the center of half-open cage and the other one Cr atom on the exterior. 9A, as the most stable structure, has doublet spin multiplicity (1 μ_B), and the metastable structure 9B, with the same spin moment as 9A, is only 0.03 eV higher in energy, while 9C with sextet spin multiplicity (5 μ_B), is less stable than 9A by 0.21 eV. The VDEs of 9A, 9B and 9C from theoretical calculation are 3.02, 2.88 and 2.90 eV, respectively, in which the VDE of 9A is closer to the experimental measurement (3.0 eV). Since isomer 9B is nearly energetically degenerated with 9A, the simulated photoelectron spectra for both 9A and 9B are presented in figure 2; both spectra share some feature with the experimental one. Hence, we speculate that isomers 9A and 9B probably coexist in experiment, while 9C with higher energy is unlikely to exist.

4.8. $Cr_2Ge_{10}^-$

The most stable isomer of $Cr_2Ge_{10}^-$, 10A in figure 1 with doublet spin multiplicity (1 μ_B), is a closed-cage structure with one Cr atom encapsulated in the center and another one Cr atom on the vertex of rectangular pyramid. 10B (quartet spin multiplicity, i.e. total spin moment of 3 μ_B) is a distorted pentagonal antiprism with one Cr atom in the cage center, and 10C (doublet spin multiplicity with total spin moment of 3 μ_B) is a pentagonal prism with one interior Cr atom and another one on vertex. They are 0.14 and 0.24 eV higher in energy than the ground state structure 10A, respectively. The calculated VDEs are 2.44, 2.60 and 2.93 eV for 10A, 10B and 10C, respectively, both 10A and 10B are close to the experimental VDE (2.5 eV). From figure 2, we can see that the simulated spectra of isomers 10A and 10B agree well with the experiment, suggesting that both isomers may coexist in experiment, whereas 10C can be ruled out.

4.9. $Cr_2Ge_{11}^-$

With respect to the $Cr_2Ge_{11}^-$ cluster, the lowest-energy isomer (11A in figure 1) can be described as a hexagonal pyramid capped on a pentagonal pyramid to form an unclosed cage structure, stuffed with one Cr atom at the cage center. 11B is a pentagonal prism capped with one Ge atom, which is 0.27 eV higher than 11A in energy. Both 11A and 11B exhibit doublet spin multiplicity (1 μ_B). Their theoretical VDEs are 3.11 and 3.20 eV for 11A and 11B, respectively, both being close to the experiment value (3.17 eV). After comparing the simulated spectra with experimental one in figure 2, one can see that 11A is consistent with the experimental spectra better, but the contribution from 11B cannot be entirely ruled out.

4.10. $Cr_2Ge_{12}^-$

For the $Cr_2Ge_{12}^-$ cluster, the most stable isomer (12A in figure 1) can be considered as a Cr-centered hexagonal antiprism capped with one Cr atom. 12A with doublet spin multiplicity (1 μ_B) is 0.18 eV lower than the quartet (3 μ_B) isomer shown as 12B. While 12C (doublet spin multiplicity with total spin moment of 1 μ_B) with configuration of a closed cage structure with one pentagonal bipyramid on top and a hexagonal pyramid on the bottom is 0.52 eV higher than 12A in energy. The theoretical VDEs for 12A, 12B and 12C are 2.55, 2.70 and 2.72 eV, respectively, which are generally smaller than experimental VDE of 3.08 eV. After comparing the simulated and experimental photoelectron spectra in figure 2, the weak peaks at about 2.5 eV in experiment are more likely contributed by 12A and the trend of 12A is closer to experiment. Meanwhile, 12B may coexist in experiment, but 12C is much higher in energy than 12A and can be excluded.

4.11. $Cr_2Ge_{13}^-$

The lowest-energy structure of $Cr_2Ge_{13}^-$ (13A in figure 1) is based on the 12A configuration, i.e. one extra Ge atom added on the top of 12A to form a C_s symmetric structure which has doublet spin multiplicity (1 μ_B). The metastable structure of 13B, 0.12 eV higher than 13A, is constructed by adding one Ge atom on the bottom of 12A to form a closed cage structure which owns the quartet spin multiplicity (3 μ_B). The theoretical VDEs are 2.77 and 2.83 eV for 13A and 13B, respectively. Their comparable VDEs are both close to the experimental VDE (3.00 eV). From comparison between the simulated photoelectron spectra and experiment in figure 2, both 13A and 13B may contribute to the experimental features. As a result, the broadening experimental photoelectron spectrum of $Cr_2Ge_{13}^-$ is probably contributed by the two co-existing isomers 13A and 13B.

4.12. $Cr_2Ge_{14}^-$

The low-lying isomers of $Cr_2Ge_{14}^-$ cluster (14A and 14B in figure 1) can be seen as four extra Ge atoms added on the top of one pentagonal prism which is decorated by one Cr atom at the center of the cage and the other Cr atom on the vertex. Both 14A and 14B have C_s symmetry and doublet spin multiplicity (1 μ_B), while 14B is less stable than 14A by 0.21 eV. The theoretical VDEs are 3.45 and 3.58 eV for 14A and 14B, respectively, both of them are substantially larger than the experimental value (2.94 eV). However, the general trend of the main peaks can be reproduced by both of 14A and 14B. Thus, we speculate the two isomers 14A and 14B coexist in experiment. While 14C and 14D (isostructural with 14A but with quartet spin multiplicity of 3 μ_B) are much higher in energy than isomer 14A by 0.58 and 0.62 eV, respectively (their structures are shown as insets of figure S2). Since the

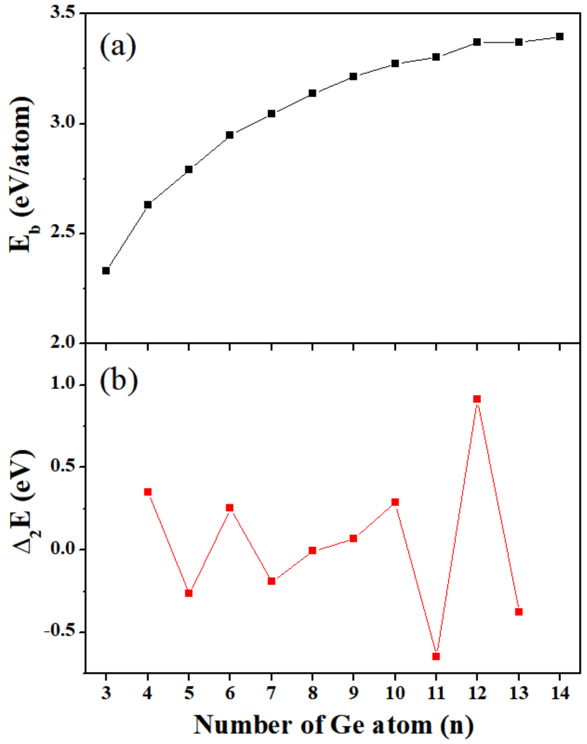

Figure 3. (a) Binding energies defined by $E_b = [2E(\mathrm{Cr_{atom}}) + nE(\mathrm{Ge_{atom}}) - E(\mathrm{Cr_2Ge}_n)]/(n+2)$; (b) second-order of energy differences of cluster energies defined by $\Delta_2 E = E(n+1) + E(n-1) - 2E(n)$ of $\mathrm{Cr_2Ge}_n^-$ $(n = 3-14)$ clusters.

first weak shoulder in experimental spectra is reproduced by the simulated spectra of isomer 14D, the contribution of isomer 14D still cannot be ruled out, while 14C unlikely exists in the experiment.

To briefly summarize, the small sized clusters, e.g. $n = 3$–8 of $\mathrm{Cr_2Ge}_n^-$ clusters have relatively sharp peaks; when the clusters get bigger, the experimental spectral features become very broad and some peaks overlap with each other. The overlapping of the experimental spectral peaks is partly caused by the complex electronic states and vibrational states of the clusters. Moreover, the experimental spectrum is probably contributed by the electronic states of multiple isomers for larger clusters $\mathrm{Cr_2Ge}_n^-$ ($n = 9$–14), i.e. the combination of the simulated spectra of the low-lying isomers reproduce the experimental spectra.

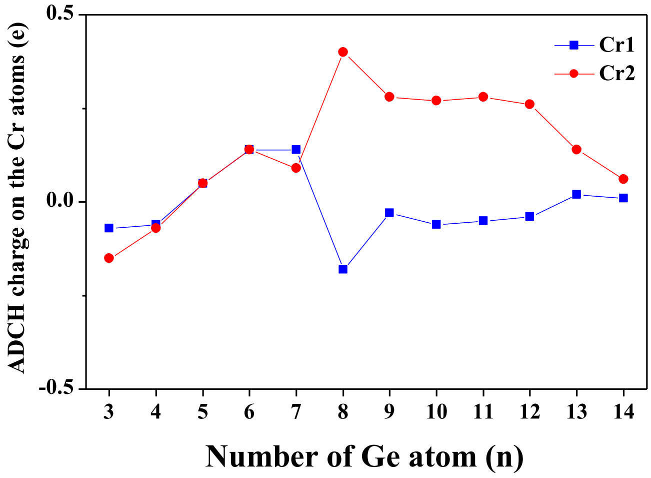

Figure 4. ADCH charge on the two Cr atoms of the ground state structures of $\mathrm{Cr_2Ge}_n^-$ ($n = 3$–14) clusters.

Table 2. Spin moment on each Cr atom for ground state structure of $\mathrm{Cr_2Ge}_n^-$ ($n = 3$–14) cluster, the total magnetic moment for two Cr toms (μ_{Cr}) and each cluster (μ_{T}). All magnetic moments are in μ_{B}.

	Spin			
Clusters	$\mathrm{Cr_1}$	$\mathrm{Cr_2}$	μ_{Cr}	μ_{T}
$\mathrm{Cr_2Ge_3^-}$	4.0	−3.7	0.3	1
$\mathrm{Cr_2Ge_4^-}$	−1.9	2.6	0.7	1
$\mathrm{Cr_2Ge_5^-}$	0.5	0.5	1	1
$\mathrm{Cr_2Ge_6^-}$	0.3	0.3	0.6	1
$\mathrm{Cr_2Ge_7^-}$	1.1	−0.5	0.6	1
$\mathrm{Cr_2Ge_8^-}$	−1.0	2.2	1.2	1
$\mathrm{Cr_2Ge_9^-}$	−0.04	1.4	1.4	1
$\mathrm{Cr_2Ge_{10}^-}$	1.4	−1.3	0.1	1
$\mathrm{Cr_2Ge_{11}^-}$	−0.7	1.4	0.7	1
$\mathrm{Cr_2Ge_{12}^-}$	−0.7	1.7	0.7	1
$\mathrm{Cr_2Ge_{13}^-}$	−0.8	1.9	1.1	1
$\mathrm{Cr_2Ge_{14}^-}$	−0.3	1.0	0.7	1

5. Discussion

Overall, the ground-state structures of the anionic clusters $\mathrm{Cr_2Ge}_n$ tend to form Cr–Cr bond, rather than being separated, similar to the previous case of $\mathrm{Fe_2Ge}_n^-$ $(3 \leqslant n \leqslant 12)$ [42]. For large clusters with $n \geqslant 9$, one Cr atom is encapsulated to form a polyhedral cage-like structure. For the smallest $\mathrm{Cr_2Ge}_n^-$ clusters ($n = 3$–5), their structures can be seen as a Cr atom substituting one of the germanium atoms in the corresponding neutral CrGe_{n+1} clusters, which have been investigated by Kapila *et al* [26] and Dhaka *et al* [44]. While for $\mathrm{Cr_2Ge}_n^-$ $(n \geqslant 6)$, the fundamental frames of the ground-state structures are basically different from those of CrGe_{n+1} clusters. Although little is known about double Cr atoms doped Ge_n clusters, doped silicon clusters have received more attention, i.e. the small $\mathrm{Cr_2Si}_n$ ($n = 1$–8) clusters have been studied [78]. After comparison of the lowest-energy structures of $\mathrm{Cr_2Ge}_n^-$ and $\mathrm{Cr_2Si}_n^-$ $(n \leqslant 8)$, their structures are similar except for $n = 4$ (the ground state structure of $\mathrm{Cr_2Si_4^-}$ is the metastable structure of $\mathrm{Cr_2Ge_4^-}$) and $n = 8$. On the other hand, molybdenum locates in the same group as chromium in the periodic table, and $\mathrm{Mo_2Ge}_n$ ($n = 9$–15) clusters have been studied by Wang *et al* [40]. We find that these two kinds of clusters share the same ground state structures at $n = 11$, 12 and 13, while $\mathrm{Mo_2Ge_{14}}$ exhibits the same basal pentagonal prism. Generally, the structural evolution of $\mathrm{Cr_2Ge}_n^-$ is similar to that of $\mathrm{Mo_2Ge}_n$ cluster for $n \geqslant 9$.

The energetic stability can be characterized by the size-dependent binding energy and second-order of energy differences of cluster energies in figures 3(a) and (b); the former is defined by $E_b = [2E(\mathrm{Cr_{atom}}) + nE(\mathrm{Ge_{atom}}) - E(\mathrm{Cr_2Ge}_n)]/(n+2)$, in which the $E(\mathrm{Cr_{atom}})$ and $E(\mathrm{Ge_{atom}})$ are the total

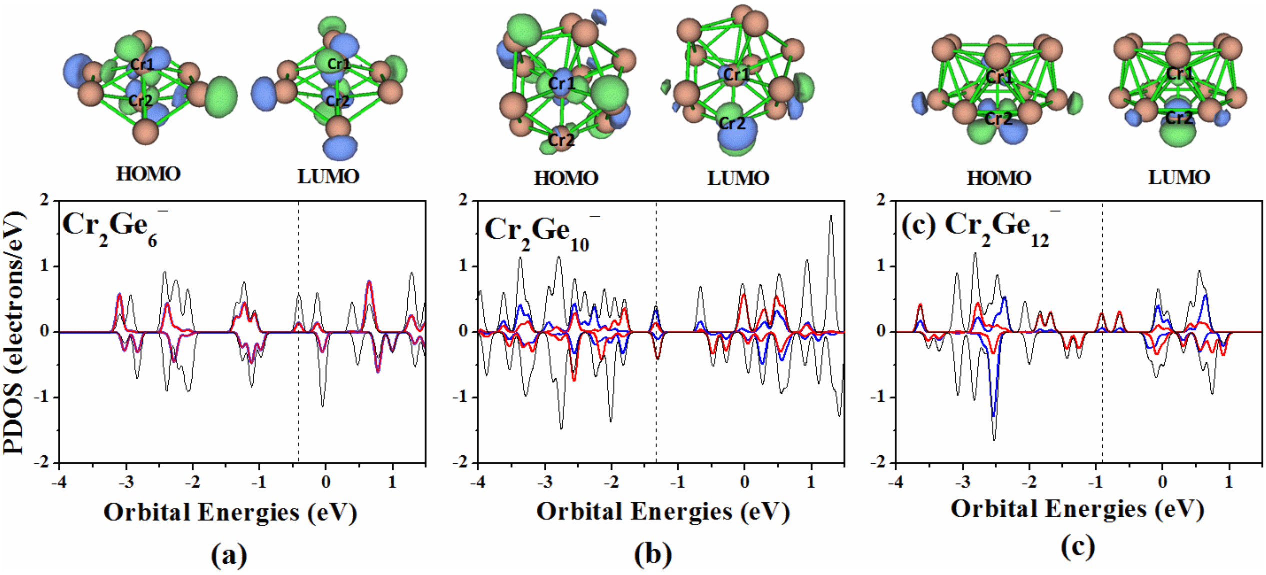

Figure 5. Calculated partial density of states (PDOS) for spin-up and spin-down states of (a) $Cr_2Ge_6^-$, (b) $Cr_2Ge_{10}^-$ and (c) $Cr_2Ge_{12}^-$ and the corresponding HOMO and LUMO illustrative motifs on top (the brown balls represent the atoms and Cr_1 and Cr_2 locations are marked). Blue and red curves show *d*-orbitals of the Cr_1 atom and Cr_2 atom, respectively, while black curves represent the *p*-orbitals of the Ge atoms. The dashed lines refer to HOMO energy.

energy of single atom in the ground spin state, i.e. Cr atom in septet and Ge atom in singlet state, respectively; and the latter is defined by $\Delta_2 E = E(n+1) + E(n-1) - 2E(n)$, where $E(n)$ represents total energy of $Cr_2Ge_n^-$ ($n = 3$–14) cluster. The binding energy increases from 2.33 to 3.39 eV/atom with cluster size of $Cr_2Ge_n^-$ increasing from $n = 3$ to 14, which indicates that inclusion of more Ge atoms would make the cluster structure more stable. As seen from the second-order energy differences in figure 3(b), the $Cr_2Ge_n^-$ clusters with $n = 6$, 10 and 12 are local maxima (magic number size) and the relatively higher stability can be related to the higher symmetry and the formation of cage-like structure. As the representative cluster sizes at $n = 6$, 10 and 12, the correlation between the stability and magnetic behavior will be discussed below.

To gain insight into the charge distributions of $Cr_2Ge_n^-$ clusters, we conducted the atomic dipole moment-corrected Hirshfeld population (ADCH) analyses on the most stable structures of $Cr_2Ge_n^-$ ($n = 3$–14) clusters. The ADCH charges on two Cr atoms as function of cluster size are shown in figure 4. One can see that the ADCH charge of Cr_1 atom ranges from -0.18 *e* to 0.14 *e*, while that on Cr_2 atom is in the range of -0.15 e to 0.28 *e*. For $n = 2$–7, the ADCH charges on two Cr atoms are almost the same, which is probably due to the identical Ge coordination environments of the two Cr atoms in these clusters. While from $n \geqslant 8$, the two Cr atoms begin to bond with different numbers of Ge atoms, i.e. one Cr atom locating in the center and the other one staying on the exterior location, resulting in a different charge distributions of the two Cr atoms, especially for $n = 8$–12. Because Cr atom prefer to bond with more Ge atoms, the exposed Cr atom tends to bond with the extra Ge atoms, resulting in the decreased difference of charge distribution between the two Cr atoms at $n = 13$ and 14. It seems that the ADCH charge distributions are related not only to the electronegativity difference between elements, but also associated with the structural evolution of $Cr_2Ge_n^-$ clusters, especially for the coordination environments of the two Cr atoms.

Finally, we discuss the magnetic properties of $Cr_2Ge_n^-$ ($n = 3$–14) clusters. The local spin moments of the two Cr atoms are presented in table 2, along with the total magnetic moments of two Cr atoms and the whole cluster. For all cluster sizes studied here, the total magnetic moment of each cluster is 1 μ_B, similar to the previous results of $Cr_2Si_n^-$ with $n \leqslant 8$ from DFT calculations [78]. Except for $Cr_2Ge_5^-$ and $Cr_2Ge_6^-$ with Cr–Cr ferromagnetic coupling, the two Cr atoms in most $Cr_2Ge_n^-$ clusters are coupled antiferromagnetically. As shown in table 2, the summation of the magnetic moments of two Cr atoms is not equal to the total magnetic moment of the whole cluster (1 μ_B), indicating that there exist induced magnetic moments on the Ge atoms.

To further explore the interaction between two Cr atoms and Ge atoms, we plot PDOS of $Cr_2Ge_6^-$, $Cr_2Ge_{10}^-$ and $Cr_2Ge_{12}^-$ as representatives in figure 5. Also, the total density of states (TDOS) of pure Ge_n clusters, $n = 6$, 10 and 12 as representatives are compared with the Cr_2-doped ones in figure S3 of supplementary material. We can see that the doped Cr atoms make the frontier orbitals levels denser and thus influence the HOMO-LUMO states. To focus on how the two Cr atoms of different environment interact with Ge atoms. In figure 5, we name two Cr atoms according to their location as Cr_1 (located at interior site) and Cr_2 (located on the outer shell) to analyze their interaction with Ge atoms. For $Cr_2Ge_{10}^-$ and $Cr_2Ge_{12}^-$, the *d*-orbital occupations of two Cr atoms are distinctly different, as seen from figures 5(b) and (c), respectively. For $Cr_2Ge_{10}^-$, the *d*-orbitals of Cr_1 atom (blue solid line) overlap with Ge-*p* orbitals are comparable to that of Cr_2 atom (red solid line) and the spin-up state of Cr_2-*d* orbitals mainly overlap with Ge-*p* orbitals, resulting in the negative spin moment on Cr_2 atom and positive spin moment on Cr_1 atom, respectively. To the contrary, $Cr_2Ge_{12}^-$ cluster has negative spin moment of Cr_1 and positive value of Cr_2 atom (see table 2). The plots of HOMO and LUMO orbitals directly demonstrate that the main contribution of frontier orbitals originates from Cr atoms, verifying that the total magnetic moment of the clusters is mainly from two Cr atoms and partially from the induced magnetic moment of Ge atoms. An exceptional case is $Cr_2Ge_6^-$ with two equivalent Cr atoms. As shown in figure 5(a), the *d* orbitals of two Cr atoms exhibit the same interaction with Ge-*p* orbitals, which explain the identical magnetic moment (0.3 μ_B) of two Cr atoms and their ferromagnetic interaction. The magnetic interaction between the two TM atoms in current systems is distinctly different from that of Fe_2Ge_n ($n = 2$–12) cluster shown in our previous study [42].

Our findings indicate that the magnetic coupling behavior mainly relies on charge transfer and coordination environment of the two TM atoms. More specifically, after being doped inside Ge_n cluster, one Cr atom acts as electron donor and the other one as accepter, whereas both doped Fe atoms are electron donors. According to our present finding, one can design different magnetic clusters or cluster-assembled materials by introducing different transition-metal dopant atoms. In particular, the stable antiferromagnetic interaction in Cr_2Ge_n clusters with a relatively wide size range may find potential application in giant magnetoresistance devices as the spintronic devices are continuously reduced in size [79, 80].

6. Conclusions

In summary, we have systematically investigated the structural evolution, electronic and magnetic properties of double-Cr atom doped Ge_n ($3 \leqslant n \leqslant 14$) anionic clusters. Overall, the simulated photoelectron spectra reproduce the experimental spectra reasonably well. The structural evolution from bipyramid-based geometry to polyhedral cage-like structure with one interior Cr atom is identified. The two Cr atoms in $Cr_2Ge_n^-$ clusters tend to form a Cr–Cr bond and occupy the high coordination sites to interact with more Ge atoms. Among all cluster sizes, $Cr_2Ge_6^-$, $Cr_2Ge_{10}^-$ and $Cr_2Ge_{12}^-$ are relatively more stable. All $Cr_2Ge_n^-$ clusters considered possess a total magnetic moment of 1 μ_B and most of them exhibit Cr–Cr antiferromagnetic interaction, except for $Cr_2Ge_5^-$ and $Cr_2Ge_6^-$ with the same ligand field for two Cr atoms. Importantly, we note that the $Cr_2Ge_n^-$ cluster is the first kind of transition-metal doped semiconductor clusters that exhibit relatively stable antiferromagnetism within a wide size range. These results provide a guidance for the future designed of cluster-assembled materials with different magnetic functionality.

Acknowledgments

This work was supported by the National Natural Science Foundation of China (11574040, 21103202, 11604039), the Fundamental Research Funds for the Central Universities of China (DUT15RC(3)099, DUT18LK07) and the Supercomputing Center of Dalian University of Technology. X C Z was supported by University of Nebraska-Lincoln Holland Computing Center.

Supplementary material

More details of theoretical method. The experimental photoelectron spectra in figure S1. The simulated photoelectron spectra of isomers with higher energies compared with the experimental ones in figure S2. The TDOS of the representatives in figure S3. The detachment energies from transformation of excited energies using TDDFT method compared with the experimental results in table S1. The Cartesian coordinates for all isomers of $Cr_2Ge_{3-14}^-$ clusters in table S2.

ORCID iDs

Jijun Zhao https://orcid.org/0000-0002-3263-7159
Xiao Cheng Zeng https://orcid.org/0000-0003-4672-8585

References

[1] Zhao J, Huang X, Jin P and Chen Z 2015 *Coord. Chem. Rev.* **289–90** 315
[2] Palyanov Y N, Kupriyanov I N, Borzdov Y M and Surovtsev N V 2015 *Sci. Rep.* **5** 14789
[3] Pillarisetty R 2011 *Nature* **479** 324
[4] Jarrold M F and Bower J E 1992 *J. Chem. Phys.* **96** 9180
[5] Lu J and Nagase S 2003 *Chem. Phys. Lett.* **372** 394
[6] Singh A K, Kumar V and Kawazoe Y 2005 *Eur. Phys. J.* D **34** 295
[7] Singh A K, Kumar V and Kawazoe Y 2005 *Phy. Rev.* B **71** 075312
[8] Neukermans S, Wang X, Veldeman N, Janssens E, Silverans R E and Lievens P 2006 *Int. J. Mass Spectrom.* **252** 145
[9] Furuse S, Koyasu K, Atobe J and Nakajima A 2008 *J. Chem. Phys.* **129** 064311
[10] Atobe J, Koyasu K, Furuse S and Nakajima A 2012 *Phys. Chem. Chem. Phys.* **14** 9403
[11] Wang J and Han J-G 2006 *J. Phys. Chem.* A **110** 12670
[12] Bandyopadhyay D and Sen P 2010 *J. Phys. Chem.* A **114** 1835
[13] Wang J and Han J-G 2005 *J. Chem. Phys.* **123** 244303
[14] Tai T B and Nguyen M T 2011 *J. Phys. Chem.* A **115** 9993
[15] Wang J, Ma L, Zhao J and Wang G 2008 *J. Phys.: Condens. Matter* **20** 335223
[16] Deng X-J, Kong X-Y, Xu H-G, Xu X-L, Feng G and Zheng W-J 2015 *J. Phys. Chem.* C **119** 11048
[17] Deng X J, Kong X Y, Xu X L, Xu H G and Zheng W J 2014 *Chemphyschem* **15** 3987
[18] Jin Y, Lu S, Hermann A, Kuang X, Zhang C, Lu C, Xu H and Zheng W 2016 *Sci. Rep.* **6** 30116
[19] Deng X-J, Kong X-Y, Xu X-L, Xu H-G and Zheng W-J 2014 *RSC Adv.* **4** 25963
[20] Lu S-J, Hu L-R, Xu X-L, Xu H-G, Chen H and Zheng W-J 2016 *Phys. Chem. Chem. Phys.* **18** 20321
[21] Deng X-J, Kong X-Y, Liang X, Yang B, Xu H-G, Xu X-L, Feng G and Zheng W-J 2017 *J. Chem. Phys.* **147** 234310
[22] Tang C, Liu M, Zhu W and Deng K 2011 *Comput. Theor. Chem.* **969** 56
[23] Kapila N, Jindal V K and Sharma H 2011 *Physica* B **406** 4612
[24] Li J, Wang G, Yao C, Mu Y, Wan J and Han M 2009 *J. Chem. Phys.* **130** 164514

[25] Wang J, Zhao J, Ma L, Wang B and Wang G 2007 *Phys. Lett.* A **367** 335

[26] Kapila N, Garg I, Jindal V K and Sharma H 2012 *J. Magn. Magn. Mater.* **324** 2885

[27] Pavlyukh Y and Hübner W 2004 *Phys. Rev.* B **70** 245434

[28] Tsui F, He L, Ma L, Tkachuk A, Chu Y S, Nakajima K and Chikyow T 2003 *Phys. Rev. Lett.* **91** 177203

[29] Goswami R, Kioseoglou G, Hanbicki A T, Jonker B T and Spanos G 2004 *Acta Mater.* **52** 2419

[30] Kioseoglou G, Hanbicki A T, Li C H, Erwin S C, Goswami R and Jonker B T 2004 *Appl. Phys. Lett.* **84** 1725

[31] Li A P *et al* 2007 *Phys. Rev.* B **75** 201201

[32] Bihler C, Jaeger C, Vallaitis T, Gjukic M, Brandt M S, Pippel E, Woltersdorf J and Gösele U 2006 *Appl. Phys. Lett.* **88** 112506

[33] Palagin D, Teufl T and Reuter K 2013 *J. Phys. Chem.* C **117** 16182

[34] Xiao R, Kuz'min M D, Koepernik K and Richter M 2010 *Appl. Phys. Lett.* **97** 232501

[35] Wang J, Ma L, Zhao J, Wang G, Chen X and Bruce King R 2008 *J. Chem. Phys.* **129** 044908

[36] Ji W and Luo C 2012 *Int. J. Quantum Chem.* **112** 2525

[37] Kumar V and Kawazoe Y 2003 *Phys. Rev. Lett.* **90** 055502

[38] Huang X, Xu H G, Lu S, Su Y, King R B, Zhao J and Zheng W 2014 *Nanoscale* **6** 14617

[39] Xia X X, Hermann A, Kuang X Y, Jin Y Y, Lu C and Xing X D 2016 *J. Phys. Chem.* C **120** 677

[40] Wang J and Han J-G 2008 *J. Phys. Chem.* A **112** 3224

[41] Han J-G, Zhao R-N and Duan Y 2007 *J. Phys. Chem.* A **111** 2148

[42] Liang X, Deng X, Lu S, Huang X, Zhao J, Xu H, Zheng W and Zeng X C 2017 *J. Phys. Chem.* C **121** 7037

[43] Hou X-J, Gopakumar G, Lievens P and Nguyen M T 2007 *J. Phys. Chem.* A **111** 13544

[44] Dhaka K and Bandyopadhyay D 2015 *RSC Adv.* **5** 83004

[45] Mahtout S and Tariket Y 2016 *Chem. Phys.* **472** 270

[46] Xu H-G, Zhang Z-G, Feng Y, Yuan J, Zhao Y and Zheng W 2010 *Chem. Phys. Lett.* **487** 204

[47] Zhao J J, Shi R L, Sai L W, Huang X M and Su Y 2016 *Mol. Simul.* **42** 809

[48] Zhao J and Xie R-H 2004 *J. Comput. Theor. Nanosci.* **1** 117

[49] Sai L, Zhao J, Huang X and Wang J 2012 *J. Nanosci. Nanotechnol.* **12** 132

[50] Sai L, Tang L, Zhao J, Wang J and Kumar V 2011 *J. Chem. Phys.* **135** 184305

[51] Huang X, Lu S-J, Liang X, Su Y, Sai L, Zhang Z-G, Zhao J, Xu H-G and Zheng W 2015 *J. Phys. Chem.* C **119** 10987

[52] Huang X, Su Y, Sai L, Zhao J and Kumar V 2015 *J. Cluster Sci.* **26** 389

[53] Hong L, Wang H, Cheng J, Huang X, Sai L and Zhao J 2012 *Comput. Theor. Chem.* **993** 36

[54] Wu X, Lu S-J, Liang X, Huang X, Qin Y, Chen M, Zhao J, Xu H-G, King R B and Zheng W 2017 *J. Chem. Phys.* **4** 146

[55] Kresse G and Furthmüller J 1996 *Phys. Rev.* B **54** 11169

[56] Kresse G and Joubert D 1999 *Phys. Rev.* B **59** 1758

[57] Perdew J P, Burke K and Ernzerhof M 1996 *Phys. Rev. Lett.* **77** 3865

[58] Frisch M *et al* 2013 Gaussian 09, revision D.01 (Wallingford, CT: Gaussian Inc.)

[59] Lu T and Chen F 2012 *J. Comput. Chem.* **33** 580

[60] Lu T and Chen F 2012 *J. Theor. Comput. Chem.* **11** 163

[61] Tozer D J and Handy N C 1998 *J. Chem. Phys.* **108** 2545

[62] Akola J, Manninen M, Häkkinen H, Landman U, Li X and Wang L-S 1999 *Phys. Rev.* B **60** R11297

[63] Lu S-J, Xu H-G, Xu X-L and Zheng W-J 2017 *J. Phys. Chem.* C **121** 11851

[64] Akola J, Manninen M, Hakkinen H, Landman U, Li X and Wang L-S 2000 *Phys. Rev.* B **62** 13216

[65] Patton D C, Porezag D V and Pederson M R 1997 *Phys. Rev.* B **55** 7454

[66] Desmarais N, Reuse F and Khanna S 2000 *J. Chem. Phys.* **112** 5576

[67] Ruiz-Díaz P, Ricardo-Chávez J, Dorantes-Dávila J and Pastor G 2010 *Phys. Rev.* B **81** 224431

[68] Cheng H and Wang L-S 1996 *Phys. Rev. Lett.* **77** 51

[69] Bondybey V and English J 1983 *Chem. Phys. Lett.* **94** 443

[70] Casey S M and Leopold D G 1993 *J. Phys. Chem.* **97** 816

[71] Michalopoulos D, Geusic M, Hansen S, Powers D and Smalley R 1982 *J. Phys. Chem.* **86** 3914

[72] Hilpert K and Ruthardt R 1987 *Ber. Bunsenges. Phys. Chem.* **91** 724

[73] Su C-X, Hales D A and Armentrout P B 1993 *Chem. Phys. Lett.* **201** 199

[74] Simard B, Lebeault-Dorget M-A, Marijnissen A and Ter Meulen J 1998 *J. Chem. Phys.* **108** 9668

[75] Froben F and Schulze W 1985 *Surf. Sci.* **156** 765

[76] Hunter J, Fye J, Jarrold M and Bower J 1994 *Phys. Rev. Lett.* **73** 2063

[77] Arnold C C, Xu C, Burton G R and Neumark D M 1995 *J. Chem. Phys.* **102** 6982

[78] Robles R, Khanna S N and Castleman A W 2008 *Phys. Rev.* B **77** 235441

[79] Baibich M N, Broto J M, Fert A, Van Dau F N, Petroff F, Etienne P, Creuzet G, Friederich A and Chazelas J 1988 *Phys. Rev. Lett.* **61** 2472

[80] Chappert C, Fert A and Van Dau F N 2007 *Nat. Mater.* **6** 813